Theoretical Chemistry Accounts (2018) 137:26
https://doi.org/10.1007/s00214-018-2202-7

REGULAR ARTICLE

Long-range exchange limit and dispersion in pure silica zeolites

Angel Albavera-Mata[1] · Claudio M. Zicovich-Wilson[2] · José L. Gázquez[3] · S. B. Trickey[4] · Alberto Vela[1]

Received: 6 October 2017 / Accepted: 16 January 2018

Abstract
The roles of the large exchange dimensionless gradient limit, $s \to \infty$, with $s = |\nabla n(\boldsymbol{r})| / \left(2k_{\mathrm{f}}(\boldsymbol{r}) n(\boldsymbol{r})\right)$, $k_{\mathrm{f}} = \left(3\pi^2 n(\boldsymbol{r})\right)^{1/3}$, and of dispersion interactions computed by Grimme's scheme in the context of solids are considered. Two families of recently developed generalized gradient approximation exchange functionals in combination with a suitably calibrated dispersion contribution are studied. Furthermore, the effects of changing the correlation functional or including exact exchange in the calculations also are explored. The results indicate that the large exchange dimensionless gradient limit has a small influence and that the most important contribution for a better description of the structure and energetics of porous materials is dispersion. The functional that provides best overall agreement with the experimental stability trend of a large set of pure silica zeolites is an exchange functional (denoted lsRPBE) based on the modified version of PBE, the exchange functional RPBE, corrected to satisfy the large exchange dimensionless limit, combined with PBE correlation and including a calibrated Grimme dispersion contribution. It outperforms any of the functionals that include exact exchange which were tested. Remarkably, the simple local density approximation does almost as well.

Keywords Zeolites · DFT · Large dimensionless exchange gradient · van der Waals · Dispersion

1 Introduction

Zeolites are among the most versatile materials for possible technological applications because of their diverse physical and chemical properties, including cell size, shape, cavities, surface area, presence of heteroatoms, and multiple structures [1]. The many possible combinations of these make zeolites an enticing option for employment as catalysts in petroleum technology [2–4] and chemical reactions [5–7], in the physisorption of industrial gas emissions [8–10], or as molecular sieve adsorbents [11]. Despite their popularity, zeolites are not an easily definable family of crystalline solids. One criterion to distinguish them from denser tectosilicates is the framework density. Pure silica zeolites exhibit high porosity, hence comparatively low material density, which makes them less stable than tectosilicates, to the point that several zeolites are known to collapse after a calcination procedure [12]. Experimental and computational studies [13–16] correlating lattice energy and framework density have estimated the energetics of several silica zeolites with respect to α-quartz, their most stable phase. Additionally, the relative stability trend observed in thermochemistry experiments was described by the formation enthalpy of that family of materials [17]. Recently, it has

Published as part of the special collection of articles "In Memoriam of Claudio Zicovich."

Electronic supplementary material The online version of this article (https://doi.org/10.1007/s00214-018-2202-7) contains supplementary material, which is available to authorized users.

✉ Alberto Vela
avela@cinvestav.mx

[1] Departamento de Química, Centro de Investigación y de Estudios Avanzados, Av. Instituto Politécnico Nacional 2508, 07360 Ciudad de México, Mexico

[2] Facultad de Ciencias, Universidad Autónoma del Estado de Morelos, Av. Universidad 1001, 62209 Cuernavaca, Mor., Mexico

[3] Departamento de Química, Universidad Autónoma Metropolitana Iztapalapa, Av. San Rafael Atlixco 186, 09340 Ciudad de México, Mexico

[4] Quantum Theory Project, Department of Physics and Department of Chemistry, University of Florida, P.O. Box 118435, Gainesville, FL 32611-8435, USA

Published online: 29 January 2018

been shown that their structural stability is dominated by dispersive forces [18].

For understanding extended systems, a successful and commonly used computational method within density functional theory (DFT) is the Kohn–Sham (KS) procedure [19–21]. In it, all contributions to the Born–Oppenheimer (fixed nuclei) energy are known exactly either in terms of the electronic density $n(\boldsymbol{r})$, or the Kohn–Sham orbitals $\varphi_i(\boldsymbol{r})$, except for the exchange–correlation (XC) contribution. For XC, existing density functional approximations (DFAs) are designed to employ not only the ground state density $n(\boldsymbol{r})$, but also its derivatives $\nabla n(\boldsymbol{r})$, $\nabla^2 n(\boldsymbol{r})$, etc., and quantities constructed from the KS orbitals $\varphi_i(\boldsymbol{r})$, including the positive definite kinetic energy density $\tau(\boldsymbol{r}) = \frac{1}{2}\sum_i \left|\nabla\varphi_i(\boldsymbol{r})\right|^2$ and exact exchange (EXX). The dependence upon distinct functional variables constitutes the basis for the Perdew and Schmidt Jacob's ladder [22] categorization of DFAs. Its first four rungs, ascending in theoretical complexity and computational demand, are the local density approximation (LDA) [dependent only on $n(\boldsymbol{r})$], the generalized gradient approximation (GGA) [dependent on $n(\boldsymbol{r})$ and $\nabla n(\boldsymbol{r})$], the meta-GGAs (mGGA) [that additionally include $\tau(\boldsymbol{r})$ or $\nabla^2 n(\boldsymbol{r})$ dependence], and global hybrids containing an EXX contribution.

In the KS context, DFAs for X and C customarily are devised separately because of their distinct scaling and asymptotic behaviors. Nonetheless, error cancelation between X and C by design is familiar in GGAs. It is also well understood in bonding regions, because one knows that the X part accounts for the regions of overlapping densities and for some intermediate range correlation effects. However, unless specially designed to rectify the omission [23], in general, simple DFAs lack long-range correlation interactions or they unsystematically simulate them [24–27]. Multiple suggestions have been made [28–37] for improving the treatment of dispersion in the context of DFAs. Among them, Grimme's approach [38, 39] adds a semiempirical sum over atomic pair contributions of damped C_6 terms to the conventional KS energy E_{KS}. The result is a corrected energy $E_{\mathrm{KS\text{-}D}}$,

$$E_{\mathrm{KS\,-\,D}} = E_{\mathrm{KS}} - s_6 \sum_{i=1}^{N-1} \sum_{j=i+1}^{N} \frac{C_6^{ij}}{R_{ij}^6} f_{\mathrm{d}}\left(R_{ij}\right). \tag{1}$$

Here, N is the number of atoms, R_{ij} is the interatomic distance between atom i and atom j, C_6^{ij} is the dispersion coefficient for atom pair ij, and s_6 is a DFA-dependent global scaling factor. The damping function, f_{d}, avoids near singularities for small R and removes contributions for short-range interactions. It is given by

$$f_{\mathrm{d}}\left(R_{ij}\right) = \frac{1}{1 + e^{-\alpha\left(R_{ij}/R_0 - 1\right)}}, \tag{2}$$

where R_0 is the sum of atomic van der Waals radii and the value of $\alpha = 20$ provides larger corrections at intermediate distances while leaving covalent bonding situations negligibly affected. Finally, a geometric mean for the evaluation of the dispersion coefficients with the form $C_6^{ij} = \sqrt{C_6^i C_6^j}$ commonly is used since it provides better results than other plausible choices.

The question at hand is the effect upon zeolite stability of different DFA choices in combination with Grimme's dispersion correction. Our study explores a set of pure silica zeolites for which experimental data [14–16] are available. It covers three of the four Jacob's ladder rungs listed before. The first is LDA, known to be rather accurate for those solids [40] in which $n(\boldsymbol{r})$ does not vary rapidly and the widely used GGAs PW91 [41], PBE [42], its revised version RPBE [43], and the more recent lsPBE and lsRPBE families [44] (named lsX when referring to both families). The lsX functionals were designed to satisfy the 1D and 2D non-uniform scaling conditions that imply that in the large exchange dimensionless gradient limit, the exchange enhancement function must satisfy the constraint $\lim_{s\to\infty} s^{1/2} F_X(s) < \infty$. Thus, asymptotically the exchange enhancement function must decay at least as $s^{-1/2}$, a condition that was included in the constraints satisfied by PW91. The analytical forms of the lsX enhancement functions are simpler than that of PW91 and, consequently, the lsX implementation is easier and their performance (measured as cycles in the SCF and in geometry optimizations) is better. An important feature of the lsX functionals is that asymptotically their enhancement functions decay to zero, unlike PBE and RPBE, both of which go to the value of the local Lieb-Oxford bound (Figure 3 of Ref. [44]). Then, there are the fourth-rung global hybrid DFAs based upon all the aforementioned GGAs except PW91. In addition, the s_6 coefficients [Eq. (1)] were calibrated for lsX DFAs in order to include long-range interactions and compare the results with those previously obtained [18] by one of the authors, who used two different DFAs and also two distinct approaches to account for dispersion. This selection enables us to evaluate the performance of these new lsX families in periodic systems in both the presence and absence of dispersion contributions.

2 Methodology

2.1 Calibration of s_6 for lsX DFAs

The s_6 scaling factor in Eq. (1) takes a value specific to a particular DFA. To evaluate it, one needs appropriate reference sets consisting of interaction energies for a wide range of weakly interacting molecules in a variety of sizes and diverse

arrangements. Those reference calculations commonly use the CCSD(T) methodology along with extrapolation to the complete basis set limit to provide accurate non-covalent interaction energy results. Robust calibration is obtained when the data sets include the A24 [45], S26 [46], S66 [47, 48], and X40 [49] benchmarks. Those sets cover different sizes of complexes and encompass hydrogen bonds, electrostatic/dispersion, dispersion-dominated and electrostatic-dominated interactions of aliphatic hydrocarbons, aromatic rings, water, alcohols, ammines and halogens, among others.

The necessary s_6 values, shown in Table 1, were determined by a least squares fit of the interaction energies obtained from single-point energy calculations with the software package *deMon2k* [50] using the geometries and basis sets corresponding to each of the above-mentioned databases. For comparison, lsX functionals were used in combination with two correlation DFAs, namely PBE and PW91, with the set of non-empirical values of the gradient expansion coefficient μ_{PBE} [42], μ_{sol} [51], μ_{MGEA} [52], and μ_{mol} [53], denoted collectively from here onward as μ_{x}. A complete list gathering the results for all the non-covalent interaction energy differences can be found in Tables S1 and S2 in the Supplementary Material.

2.2 Hybrid DFAs

A common approach to improve upon the accuracy of a GGA is the addition of an EXX contribution to yield a fourth-rung DFA, namely global hybrids. The underpinning of hybrids lies in the relationship of the non-interacting KS reference system with the fully interacting, and hence, real system. This is done via the adiabatic connection formula [54],

$$E_{\mathrm{xc}} = \int_0^1 \mathrm{d}\lambda E_{\mathrm{xc},\lambda}, \tag{3}$$

with

$$E_{\mathrm{xc},\lambda} = \langle \Psi_\lambda | V_{\mathrm{ee}} | \Psi_\lambda \rangle - \frac{1}{2} \iint \mathrm{d}\boldsymbol{r}\mathrm{d}\boldsymbol{r}' \frac{n(\boldsymbol{r}) n(\boldsymbol{r}')}{|\boldsymbol{r} - \boldsymbol{r}'|}, \tag{4}$$

Table 1 Global scaling factor s_6, calculated using the A24, S26, S66, and X40 databases for lsPBE and lsRPBE exchange families combined with PBE and PW91 correlation DFAs. X stands for exchange and C for correlation DFAs

X	C	μ_{x}			
		sol	PBE	MGEA	mol
lsPBE	PBE	0.655	0.683	0.694	0.701
lsRPBE	PBE	0.656	0.695	0.721	0.718
lsPBE	PW91	0.677	0.685	0.694	0.698
lsRPBE	PW91	0.671	0.694	0.721	0.717

where the perturbation parameter starts in the non-interacting reference ($\lambda = 0$) and goes through a continuum of partly interacting systems, all sharing the same $n(\boldsymbol{r})$, up to the real system ($\lambda = 1$). This methodology has led to a family of adiabatic connection functionals $E_{\mathrm{xc}}^{\mathrm{hyb}}$, wherein the GGAs act as adjustable contributions in the form [55]

$$E_{\mathrm{xc}}^{\mathrm{hyb}} = E_{\mathrm{xc}}^{\mathrm{GGA}} + \frac{1}{4}\left(E_{\mathrm{x}}^{\mathrm{EXX}} - E_{\mathrm{x}}^{\mathrm{GGA}}\right). \tag{5}$$

Following the notation for PBE0 [56], a popular non-empirical hybrid DFA built upon the PBE GGA in the form of Eq. (5), and taking into account the distinct μ_{x} values used in their correlation counterpart, lsX-based hybrid DFAs are designated as lsPBE0, lsPBEsol0, lsPBE$_{\mathrm{MGEA}}$0, and lsPBEmol0, and likewise with lsRPBE. To maintain their non-empirical nature, they all utilize 25% of EXX, *i.e.*, Eq. (5).

2.3 Computational details

Plane waves are the first and natural choice as basis functions for KS calculations on periodic systems, not only because of Bloch's theorem, but also because the addition of functions with shorter wavelengths, up to a cutoff, systematically improves the basis. However, when compared to Gaussian-type basis functions, unless pseudo-potentials are introduced, vast numbers of plane waves are needed to reach the same level of accuracy in the calculated KS total energy. Unhappily, such large basis sets adversely affect the computational cost of hybrid DFAs as it is known that plane wave calculations with global hybrids are several times more expensive than GGAs. Moreover, the standard localized Gaussian-type orbitals (GTO) centered at the nuclei, commonly used for molecular calculations, are well suited for extended solids since $n(\boldsymbol{r})$ is approximately a superposition of atomic densities. However, their diffuse tails can be inappropriate because the evaluation of the coulombic contributions is affected by their slow decay with distance, so they must be truncated or removed and the exponents of the remaining valence functions re-optimized.

A balance of *pros* and *cons* [57] between plane waves and GTOs led the KS calculations to be performed employing the ab initio periodic code *CRYSTAL14* [58] with Ahlrich's optimized triple-ζ valence basis [59] set including polarization functions (TZVP). In several periodic systems, it has been shown [18, 60, 61] to be nearly free of basis set superposition error (BSSE). Production of overly short bond distances in weakly bound systems has been attributed to BSSE, thereby potentially masking any deficiencies in DFAs for the description of these interactions [18, 62].

Calculations with dispersive terms were done with the s_6 scaling factors from Table 1 and also with a mean $s_6 = 0.70$ used for comparison. To achieve high-accuracy results, the tolerances for the bielectronic integrals were set to their

default values with the exception of the overlap threshold for Coulomb integrals and the pseudo-overlap, which were fixed to 10^{-8} and 10^{-25}, respectively. Optimizations on both atomic positions and cell parameters with analytic gradient techniques under the corresponding space group symmetry constraints through a *quasi*-Newton algorithm using Broyden–Fletcher–Goldfarb–Shanno (BFGS) methodology for Hessian updating and the trust radius strategy for step length control [58] were employed. The rest of the computational parameters were left to their default values.

All silica zeolites whose formation enthalpies have been reported in Refs. [14–16] were considered, with the exception of the porous silica denoted as BEA. The experimental values concern the enthalpy of transition ΔH_x, from α-quartz as reference system to a specific zeolite framework. In the results presented here, we assume that the *PV* contribution is small compared to the electronic nuclear energy, and hence, the total energy can be taken as a good approximation to the enthalpy of transition [18].

3 Results and discussion

Different deviation indicators for the calculated molar volumes, V, and the energy differences relative to α-quartz, ΔE_c, of the silica zeolites are shown in Fig. 1 and Table S3 in the Supplementary Material. The mean absolute deviation was calculated as $\mathrm{MAD} = (1/|\mathrm{FCode}|) \sum_{i \in FCode} \left| x_i - x_i^{\mathrm{expt}} \right|$, the mean signed deviation as $\mathrm{MSD} = (1/|\mathrm{FCode}|) \sum_{i \in \mathrm{FCode}} \left(x_i - x_i^{\mathrm{expt}} \right)$, the percentage of mean absolute relative deviation as $\%\mathrm{MARD} = 100(1/|\mathrm{FCode}|) \sum_{i \in \mathrm{FCode}} \left| x_i - x_i^{\mathrm{expt}} \right| / x_i^{\mathrm{expt}}$, and the standard deviation as $\mathrm{SD} = \left[(1/|\mathrm{FCode}|) \sum_{i \in \mathrm{FCode}} \left(x_i - x_i^{\mathrm{expt}} \right)^2 \right]^{1/2}$, where x_i is the calculated property, x_i^{expt} the experimental reference, and |FCode| is the total number of frameworks considered (see Tables S4 and S5 in the Supplementary Material for a complete list of molar volumes and calculated energy differences for all DFAs and frameworks).

From the values for the MAD and MSD reported in Fig. 1 and Table S3, one can see that all DFAs overestimate V within the range 1.81–4.33 cm^3/mol, corresponding to a relative deviation of 5.25–12.57%, as shown in the %MARD column in Table S3. The minimum deviations correspond to LDA followed closely by lsPBEsol-D, PBE0-D, lsPBEsol0, and lsRPBEsol-D, while the largest deviations are obtained with lsRPBEmol using PBE and PW91 correlation. With respect to ΔE_c, all DFAs lacking dispersion correction perform better than B3LYP (except for RPBE and RPBE0), while all DFAs with dispersion do better than B3LYP-D with the sole exception of lsPBEsol-D. Also from Fig. 1 and Table S3, one can see that the MAD for the transition enthalpies spans the range 1.81–9.40 kJ/mol. In this case, LDA has the smallest deviation followed by lsRPBE-D, the first GGA with the smallest deviation, while RPBE, RPBE0, and B3LYP have the largest deviations. Figure 1 shows that PW91 and PBE have very similar trends in energetics and structural properties. Interestingly, PW91 and lsRPBE with PBE correlation have very similar behaviors, in agreement with the conclusions of Pacheco-Kato et al. [44]. On the other hand, hybridizing EXX with GGAs improves the structural description of zeolites, but corresponding improvement is not generally observed in the transition enthalpies.

Another interesting feature from the values shown in Fig. 1 is concerned with the lsX DFAs. Note that for these functionals, the rows in Fig. 1 (and Table S3) are ordered, from top to bottom, by increasing values of μ_x. The deviations in the molar volumes of all lsX DFAs increase with increasing μ_x, independently of correlation, EXX or the inclusion of dispersion corrections. Regarding the energetics, we find that for the lsX functionals without dispersion, with the exception only of lsRPBE-PW91, the deviations increase on going from μ_{sol} to μ_{mol}. In contrast with the previous trends, the deviations for the lsX-D functionals decrease, competing and in some cases performing better than functionals with EXX including dispersion, thus becoming the functionals with the most physically coherent picture of these systems. Finally, it is worth noting that the presence of the large exchange dimensionless gradient behavior improves the structural as well as the energetic description of pure silica zeolites (compare values corresponding to PBE with lsPBE (μ_x = PBE), and RPBE with lsRPBE (μ_x = PBE), all with PBE correlation).

For further analysis of the energetic trends obtained with the DFAs considered in this work, with particular emphasis upon the dispersion contribution, in Fig. 2, we depict the calculated versus experimental transition enthalpies, relative to α-quartz. Figure 2a shows that LDA gives good agreement with the experimental values. In contrast, the GGAs shown in Fig. 2a–h all give values clustered below the dotted line, *i.e.*, those DFAs underestimate the transition enthalpies. Figure 2b shows that adding EXX has a marginal effect on these energy differences, thus making no clear improvement in describing ΔE_c. The role played by including the satisfaction of the large dimensionless gradient limit in the exchange, namely, the lsX DFAs, is shown in Fig. 2c–h. Regarding the lsPBE family, it is clear in Fig. 2c–e that independent of the value of μ_x, the energy differences get closer to the experimental values, providing better values than the exchange DFAs without proper large gradient behavior. The lsRPBE family in Fig. 2f–h shows a similar improvement. Another noticeable feature observed with the lsX DFAs is that in general the spread of values of ΔE_c is smaller than those

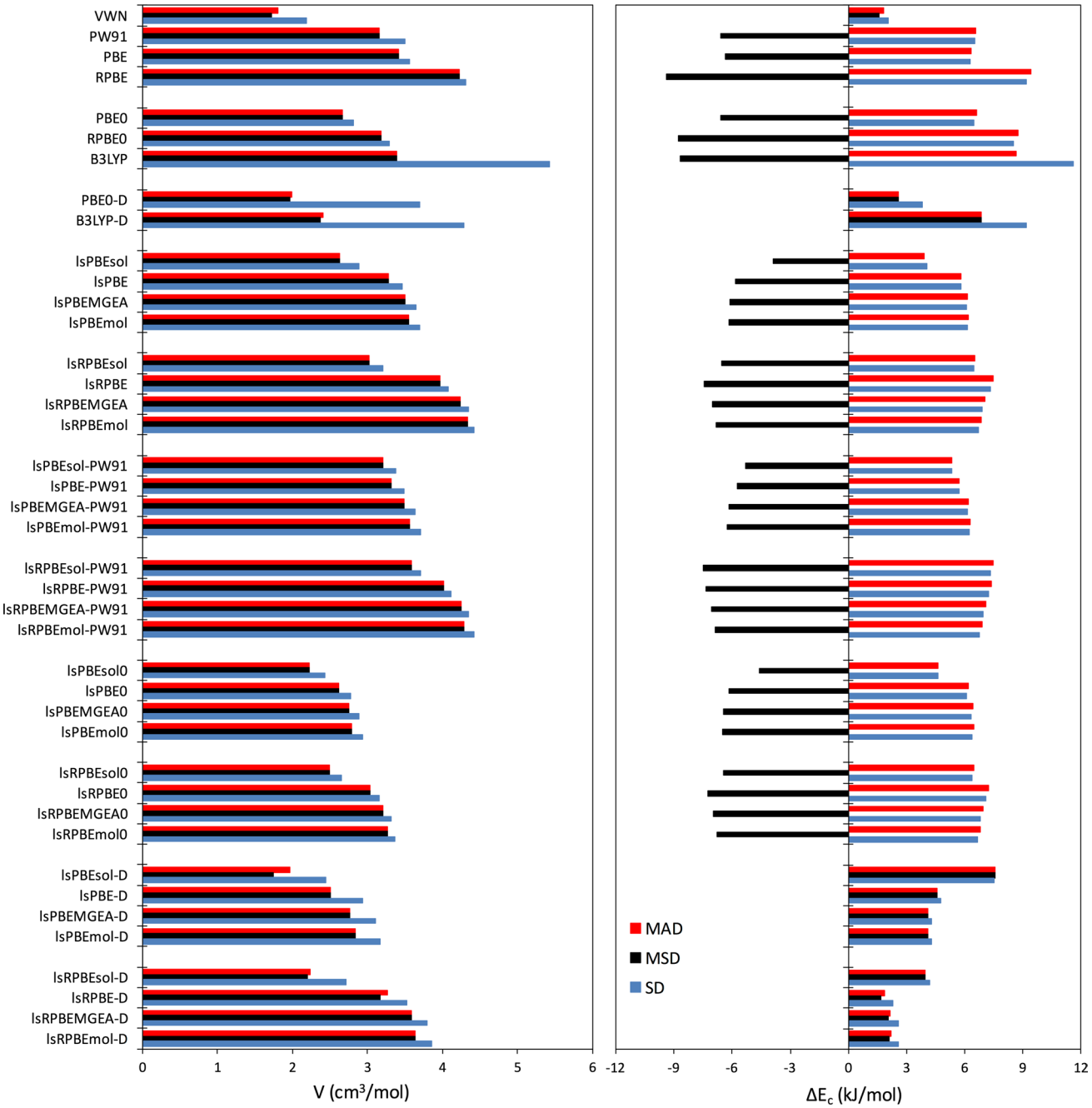

Fig. 1 Mean absolute deviation MAD, mean signed deviation MSD, and standard deviation SD, for the calculated molar volumes V, in cm^3/mol, and for the calculated energy ΔE_c, in kJ/mol, per SiO_2 unit considering different DFAs, of silica zeolites relative to α-quartz

corresponding to exchange functionals that do not have the proper large dimensionless gradient behavior. This statement is further supported by the plots in Figs. S1 to S7, available in the Supplementary Material. There one can see that the statistical correlation coefficients of the lsX families are better than those corresponding to exchange functionals without the correct large gradient behavior. To illustrate this point, the correlation coefficients obtained with DFAs without that large gradient behavior (Fig. S1) range from 0.37, corresponding to RPBE, to 0.82 for PBE0. In contrast, the lsPBE family (Figs. S2 to S4) has correlation coefficients ranging from 0.79 (lsPBEmol-PW91 in Fig. S3) to 0.9 (lsPBEsol0-PBE in Fig. S4). The reduction in the spread in values is less pronounced with the lsRPBE family. For that, the correlation coefficients go from 0.7 (lsRPBE-PBE in Fig. S5) to 0.84 (lsRPBEsol0-PBE in Fig. S7). Nevertheless, in both cases the reduction in spreading with the lsX functionals is evident.

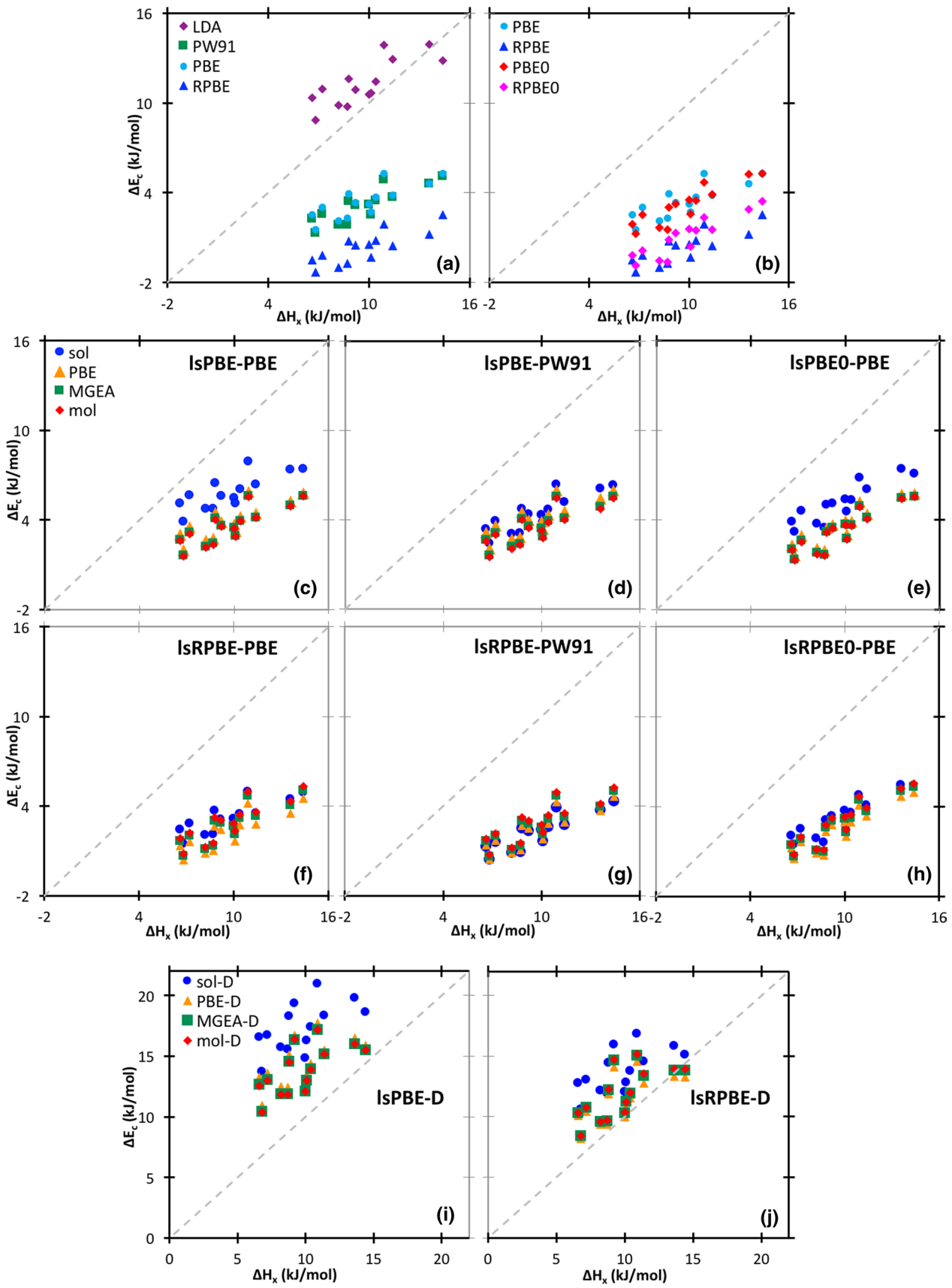
LDA
PW91
PBE
RPBE
(a)
PBE
RPBE
PBE0
RPBE0
(b)
sol
PBE
MGEA
mol
lsPBE-PBE
(c)
lsPBE-PW91
(d)
lsPBE0-PBE
(e)
lsRPBE-PBE
(f)
lsRPBE-PW91
(g)
lsRPBE0-PBE
(h)
sol-D
PBE-D
MGEA-D
mol-D
lsPBE-D
(i)
lsRPBE-D
(j)
ΔE_c (kJ/mol)
ΔH_x (kJ/mol)

◂**Fig. 2** Comparison between calculated energy ΔE_c, and experimental enthalpy of transition ΔH_x, relative to α-quartz of all considered frameworks for **a** LDA and the three GGAs indicated in the legend, **b** the two GGAs indicated in the legend with their corresponding non-empirical hybrids, **c**–**e** lsPBE family with PBE, PW91 and the non-empirical hybrid with PBE correlation, respectively, **f**–**h** lsRPBE family with PBE, PW91, and the non-empirical hybrid with PBE correlation, respectively, **i** dispersion-corrected lsPBE-D family, and **j** dispersion-corrected lsRPBE-D family

Figure 2i, j clearly shows that the dispersion correction is required to obtain an acceptable description of the energetics of pure silica zeolites from a GGA. Along with this last statement, from the data reported in Table S3, the MADs of the energies for lsPBE-D and lsRPBE-D are 1.24 and 5.59 kJ/mol below the MADs corresponding to lsPBE and lsRPBE, while the MADs for the molar volumes are 0.77 and 0.7 cm^3/mol below. In other terms, this means an improvement of 21.3 and 74.9% for the energetics versus 23.5 and 17.6% for the structural description, respectively. From these last observations, an appeal to the criterion of balance in the accuracy of the predicted structural and energetic properties of the frameworks leads to the conclusion that lsRPBE-D is the best performing DFA among those considered. That conclusion is notwithstanding that the lsPBE-D functionals are slightly better choices for the structural description than the lsRPBE-D family.

The relationship between structural and thermodynamic data commonly is correlated experimentally [16, 63] and exhibits a linear behavior with good correlation coefficients. As is clear in Fig. 3 (note the different scales), the theoretical approach showing better agreement with the observed experimental trend (Fig. 3a) is achieved via the inclusion of dispersive terms (Fig. 3c). In Fig. 3b, lsRPBEsol has the best correlation within the lsRPBE family, but a slope far away from that in Fig. 3a. Instead, the lsRPBE-D family in Fig. 3c not only exhibits a competitive correlation, but also has more realistic slopes, strengthening emphasis upon the role played by dispersion in porous materials. Since ΔH_x measures the energy involved in the formation of the framework from α-quartz, the linear correlation in Fig. 3 indicates that the formation of porous zeolites requires energy to form the cavities observed in these materials.

The dispersive corrected calculations, reported in Table 2, that use the global scaling factor value $s_6 = 0.70$ (labeled as −D*), help to compare the amount of dispersion energy contribution $E^{(dsp)}$, from the total energy E, with respect to α-quartz in the form $\%\mathrm{Disp} = [100]\left[\left(E_{zeo}^{(dsp)} - E_{qua}^{(dsp)}\right)/\left(E_{zeo} - E_{qua}\right)\right]$, enabling one to quantify the fraction of relative energy due to dispersion (see Table S6 from the Supplementary Material for further error analyses). In general, the dispersive contributions in the lsRPBE-D* family are greater than those in lsPBE-D*,

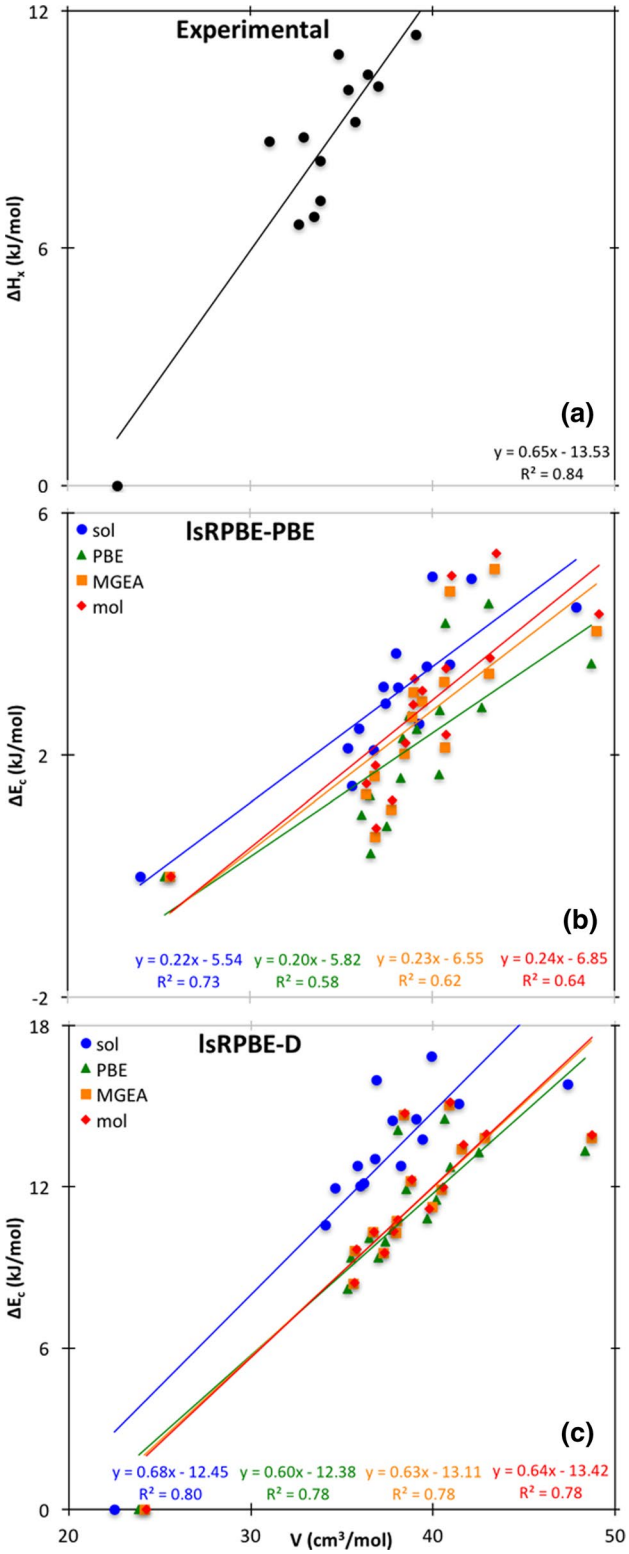

Fig. 3 Trends for **a** the experimental transition enthalpies ΔH_x, versus the experimental molar volume V, **b** the calculated energy differences ΔE_c, versus the calculated V for the dispersion-corrected lsRPBE-D family, and **c** ΔE_c vs V for lsRPBE family

Table 2 Percentage of dispersive contributions with a mean value of $s_6 = 0.70$, relative to α-quartz, for the silica zeolites considered

FCode	lsPBE-D*				lsRPBE-D*			
	sol	PBE	MGEA	mol	sol	PBE	MGEA	mol
AFI	75.3	83.8	84.8	85.1	87.0	94.5	90.2	88.3
AST	71.2	76.0	75.8	75.8	79.3	80.0	75.8	74.0
CFI	74.2	80.7	81.2	81.3	84.0	87.7	83.7	82.1
CHA	73.7	79.9	80.0	79.7	84.1	84.4	78.4	77.5
FAU	70.8	76.9	76.7	76.5	79.8	82.0	77.5	75.7
FER	79.7	88.9	89.8	90.1	92.0	99.0	94.7	92.8
IFR	66.5	76.3	78.0	77.7	78.5	85.9	81.9	80.3
ISV	68.9	72.6	72.1	71.8	75.8	74.7	70.1	68.5
ITE	76.3	84.5	85.0	85.0	88.1	92.8	87.8	85.8
MEL	79.2	90.3	91.6	91.8	93.1	102.4	99.1	97.1
MFI	78.4	90.9	92.1	92.8	93.4	104.5	100.6	98.6
MTW	77.9	87.9	88.8	89.0	91.9	100.0	95.2	93.2
MWW	75.3	81.5	81.5	81.4	85.0	86.7	81.8	80.0
STT	77.5	83.8	83.9	83.9	86.8	89.1	85.4	83.9

A color gradient is included to facilitate the reading of the table. The lowest dispersion contributions are colored in green and the highest in red

implying that lsRPBE-D* DFAs add more dispersion than the lsPBE-D* family.

The overall view reveals that all DFAs without correction for dispersion, with the exception of LDA, underestimate ΔE_c, but as dispersion corrections are included these values are no longer underestimated. This behavior approximately follows the ordering {ls(R)PBE-D, ls(R)PBE0} < ls(R)PBE < (R)PBE. See Table S5 of Supplementary Material for details.

4 Conclusions and outlook

The roles of the large exchange dimensionless gradient limit and the inclusion of damped dispersion in KS calculations of geometric and energetic properties of pure silica zeolites have been investigated.

Results show that LDA provides a good description for the structural and the energetics of these porous materials. They also show that all GGAs underestimate the energy differences, independently of including large exchange dimensionless gradient-corrected functionals, the type of correlation functional and adding exact exchange. We also show, in agreement with previous work, that the most important contribution for a better GGA-based description of these porous materials is dispersion.

We find that the best descriptions are obtained with lsRPBE-D, a combined DFA involving the novel lsRPBE functional along with the additionally calibrated scaling factor $s_6 = 0.695$ of Grimme's empirical dispersion methodology. Our investigations using different GGAs clearly indicate that when dispersion is considered, the results are in better agreement with experiment and, in most cases, outperforming global hybrids. This is relevant if one considers studying these porous materials using plane wave methodology wherein exact exchange is several times slower than GGA calculations.

Finally, parameter-free additional calculations employing non-empirical schemes, such as the one from Tkatchenko and Scheffler [37], to account for long-range van der Waals interactions are an interesting alternative to consider if one wishes to use a non-empirical DFT implementation.

5 Supplementary Material

The Supplementary Material collects complete lists with energy differences for the total 156 dimers included in the benchmarks employed for the calibration of Grimme's dispersion coefficient for the lsX families with PBE and PW91 correlation. Furthermore, detailed information about deviation indicators and the comparison between calculated molar volumes and energy differences with their corresponding experimental values for all pure silica zeolites for the exchange–correlation DFAs combinations considered in this work. Linear fits and correlation coefficients concerning experimental transition enthalpies and calculated energy differences are included for comparison.

Acknowledgements Claudio Zicovich-Wilson was an excellent scientist and human being, whose premature departure leaves us without the critical and inquisitive colleague, but mostly without the great person and friend whom we will miss forever. Calculations were performed with the computing resources provided by the Laboratorio de Supercómputo y Visualización en Paralelo from UAM-I in the cluster Yoltla,

and CGSTIC-Cinvestav facilities in the hybrid cluster Xiuhcóatl. AAM also thanks Conacyt for the PhD financial support through Grant Number 487646. JLG and AVA thank Conacyt for Grants 237045 and Fronteras 867, respectively. SBT was supported by U.S. Dept. of Energy Grant DE-SC0002139.

References

1. Baerlocher C, McCusker LB, Olson DH (2007) Atlas of zeolite framework types, 6th edn. Elsevier, Amsterdam
2. Babitz SM, Williams BA, Miller JT, Snurr RQ, Haag WO, Kung HH (1999) Appl Catal A Gen 179:71–86
3. Williams BA, Ji W, Miller JT, Snurr RQ, Kung HH (2000) Appl Catal A Gen 203:179–190
4. Tranca DC, Zimmerman PM, Gomes J, Lambrecht D, Keil FJ, Head-Gordon M, Bell AT (2015) J Phys Chem C 119:28836–28853
5. Barthomeuf D (1996) Catal Rev 38:521–612
6. Corma A (2003) J Catal 216:298–312
7. Horsley JA (1997) ChemTech 27:45–49
8. Figueroa JD, Fout T, Plasynski S, McIlvried H, Srivastava RD (2008) Int J Greenh Gas Control 2:9–20
9. Fischer M, Bell RG (2013) J Phys Chem C 117:24446–24454
10. Nour Z, Berthomieu D (2014) Mol Simul 40:33–44
11. Breck D (1974) Zeolite molecular sieves: structure, chemistry and use. Wiley, New York
12. Barrer RM, Makki MB (1964) Can J Chem 42:1481–1487
13. Momma K (2014) J Phys Condens Matter 26:103203
14. Navrotsky A, Trofymluk O, Levchenko AA (2009) Chem Rev 109:3885–3902
15. Petrovic I, Navrotsky A, Davis ME, Zones SI (1993) Chem Mater 5:1805–1813
16. Piccione PM, Laberty C, Yang SY, Camblor MA, Navrotsky A, Davis ME (2000) J Phys Chem B 104:10001–10011
17. Boerio-Goates J, Stevens R, Hom BK, Woodfield BF, Piccione PM, Davis ME, Navrotsky A (2002) J Chem Thermodyn 34:205–227
18. Roman-Roman EI, Zicovich-Wilson CM (2015) Chem Phys Lett 619:109–114
19. Kohn W, Sham LJ (1965) Phys Rev 140:1133–1138
20. Parr RG, Yang W (1989) Density functional theory of atoms and molecules. Oxford University Press, Oxford, Engalnd
21. Perdew JP, Kurth S (2003) A primer in density functional theory, vol 620. Springer lecture notes in physics. Springer, New York
22. Perdew JP, Schmidt K (2001) Density functional theory and its application to materials. AIP, Melville, New York
23. Chakarova-Kack SD, Schroder E, Lundqvist BI, Langreth DC (2006) Phys Rev Lett 96:146107
24. Jones RO, Gunnarsson O (1989) Rev Mod Phys 61:689–746
25. Klimes J, Michaelides A (2012) J Chem Phys 137:120901
26. Ruzsinszky A, Perdew JP, Csonka GI (2005) J Phys Chem A 109:11006–11014
27. Ruzsinszky A, Perdew JP, Csonka GI (2005) J Phys Chem A 109:11015–11021
28. Grafenstein J, Cremer D (2009) J Chem Phys 130:124105
29. Hermann J, Bludsky O (2013) J Chem Phys 139:034115
30. Hesselmann A (2013) J Chem Theory Comput 9:273–283
31. Hesselmann A, Jansen G (2003) Phys Chem Chem Phys 5:5010–5014
32. Kerber T, Sierka M, Sauer J (2008) J Comput Chem 29:2088–2097
33. Misquitta AJ, Jeziorski B, Szalewicz K (2003) Phys Rev Lett 91:033201
34. Osinga VP, vanGisbergen SJA, Snijders JG, Baerends EJ (1997) J Chem Phys 106:5091–5101
35. Tkatchenko A, Ambrosetti A, DiStasio RA (2013) J Chem Phys 138:074106
36. Tkatchenko A, Romaner L, Hofmann OT, Zojer E, Ambrosch-Draxl C, Scheffler M (2010) MRS Bull 35:435–442
37. Tkatchenko A, Scheffler M (2009) Phys Rev Lett 102:073005
38. Grimme S (2004) J Comput Chem 25:1463–1473
39. Grimme S (2006) J Comput Chem 27:1787–1799
40. Gunnarsson O, Lundqvist BI, Wilkins JW (1974) Phys Rev B 10:1319–1327
41. Perdew JP, Chevary JA, Vosko SH, Jackson KA, Pederson MR, Singh DJ, Fiolhais C (1992) Phys Rev B 46:6671–6687
42. Perdew JP, Burke K, Ernzerhof M (1996) Phys Rev Lett 77:3865–3868
43. Hammer B, Hansen LB, Norskov JK (1999) Phys Rev B 59:7413–7421
44. Pacheco-Kato JC, del Campo JM, Gazquez JL, Trickey SB, Vela A (2016) Chem Phys Lett 651:268–273
45. Rezac J, Hobza P (2013) J Chem Theory Comput 9:2151–2155
46. Riley KE, Hobza P (2007) J Phys Chem A 111:8257–8263
47. Rezac J, Riley KE, Hobza P (2011) J Chem Theory Comput 7:2427–2438
48. Rezac J, Riley KE, Hobza P (2011) J Chem Theory Comput 7:3466–3470
49. Rezac J, Riley KE, Hobza P (2012) J Chem Theory Comput 8:4285–4292
50. Koster AM, Geudtner G, Calaminici P, Casida ME, Dominguez VD, Flores-Moreno R, Gamboa GU, Goursot A, Heine T, Ipatov A, Janetzko F, del Campo JM, Reveles JU, Vela A, Zuniga-Gutierrez B, Salahub DR (2011) The deMon Developers. deMon2 k, Version 4, The deMon Developers, Cinvestav, Mexico City
51. Antoniewicz PR, Kleinman L (1985) Phys Rev B 31:6779–6781
52. Constantin LA, Fabiano E, Laricchia S, Della Sala F (2011) Phys Rev Lett 106:186406
53. del Campo JM, Gazquez JL, Trickey SB, Vela A (2012) J Chem Phys 136:104108
54. Gunnarsson O, Lundqvist BI (1976) Phys Rev B 13:4274–4298
55. Ernzerhof M, Burke K, Perdew JP (1996) J Chem Phys 105:2798–2803
56. Adamo C, Barone V (1999) J Chem Phys 110:6158–6170
57. Tosoni S, Tuma C, Sauer J, Civalleri B, Ugliengo P (2007) J Chem Phys 127:154102
58. Dovesi R, Orlando R, Erba A, Zicovich-Wilson CM, Civalleri B, Casassa S, Maschio L, Ferrabone M, De La Pierre M, D'Arco P, Noel Y, Causa M, Rerat M, Kirtman B (2014) Int J Quantum Chem 114:1287–1317
59. Schafer A, Huber C, Ahlrichs R (1994) J Chem Phys 100:5829–5835
60. Civalleri B, Zicovich-Wilson CM, Valenzano L, Ugliengo P (2008) CrystEngComm 10:405–410
61. Zicovich-Wilson CM, Gandara F, Monge A, Camblor MA (2010) J Am Chem Soc 132:3461–3471
62. Kristyan S, Pulay P (1994) Chem Phys Lett 229:175–180
63. Slipenyuk A, Eckert J (2004) Scripta Mater 50:39–44